Published in final edited form as:

J Bone Miner Res. 2018 June ; 33(6): 1066–1075. doi:10.1002/jbmr.3393.

Contributions of material properties and structure to increased bone fragility for a given bone mass in the UCD-T2DM rat model of type 2 diabetes

Claire Acevedo[1,2,3], **Meghan Sylvia**[1], **Eric Schaible**[4], **James L. Graham**[5,6], **Kimber L. Stanhope**[5,6], **Lionel N. Metz**[1], **Bernd Gludovatz**[7], **Ann V. Schwartz**[8], **Robert O. Ritchie**[2,9], **Tamara N. Alliston**[1], **Peter J. Havel**[5,6], and **Aaron J. Fields**[1]

[1]Department of Orthopaedic Surgery, University of California, San Francisco, CA

[2]Materials Science Division, Lawrence Berkeley National Laboratory, Berkeley, CA

[3]Department of Mechanical Engineering, University of Utah, Salt Lake City, UT, USA

[4]Experimental Systems Group, Advanced Light Source, Berkeley, CA

[5]Department of Molecular Biosciences, University of California, Davis, CA

[6]Department of Nutrition, University of California, Davis, CA

[7]School of Mechanical and Manufacturing Engineering, UNSW Sydney, NSW 2052, Australia

[8]Department of Epidemiology and Biostatistics, University of California, San Francisco, CA

[9]Department of Materials Science and Engineering, University of California, Berkeley, CA

Abstract

Adults with type 2 diabetes (T2D) have a higher fracture risk for a given bone quantity, but the mechanisms remain unclear. Using a rat model of polygenic obese T2D, we demonstrate that diabetes significantly reduces whole-bone strength for a given bone mass (micro-CT-derived BMC), and we quantify the roles of T2D-induced deficits in material properties versus bone structure, *i.e.*, geometry and microarchitecture. Lumbar vertebrae and ulnae were harvested from 6-month-old lean Sprague-Dawley rats, obese Sprague-Dawley rats, and diabetic obese UCD-T2DM rats (diabetic for 69 ± 7 days; blood glucose >200 mg/dl). Both obese rats and those with diabetes had reduced whole-bone strength for a given BMC. In obese rats, this was attributable to structural deficits, whereas in UCD-T2DM rats, this was attributable to structural deficits and to deficits in tissue material properties. For the vertebra, deficits in bone structure included thinner and more rod-like trabeculae; for the ulnae, inefficient distribution of bone mass to resist bending. Deficits in ulnar material properties in UCD-T2DM rats were associated with increased non-

Corresponding author: Aaron J. Fields, Ph.D., 513 Parnassus Avenue, S-1161, University of California, San Francisco, CA 94143-0514, USA, (415) 476-0960, fax (415) 476-1128, aaron.fields@ucsf.edu.

Author Contributions

Authors' roles: Study design: AJF. Study conduct: CA, MS, BG and AJF. PJH, JLG, and KLS were involved in the development and characterization of the UCD-T2DM rat model. Data collection: CA, MS, JLG and AJF. Data analysis: CA, ES, MS and AJF. Data interpretation: CA and AJF. Drafting manuscript: CA and AJF. Revising manuscript content: CA, JLG, KSL, LNM, AVS, PJH, ROR, TNA, and AJF. All authors approved the final version of manuscript. AJF and CA take responsibility for the integrity of the data analysis.

enzymatic crosslinking and impaired collagen fibril deformation. Specifically, small angle X-ray scattering revealed that diabetes reduced collagen fibril ultimate strain by 40%, and those changes coincided with significant reductions in the elastic, yield, and ultimate tensile properties of the bone tissue. Importantly, the biomechanical effects of these material property deficits were substantial. Prescribing diabetes-specific tissue yield strains in high-resolution finite element models reduced whole-bone strength by a similar amount (and in some cases a 3.4-fold greater amount) as the structural deficits. These findings provide insight into factors that increase bone fragility for a given bone mass in T2D; not only does diabetes associate with less biomechanically efficient bone structure, but diabetes also reduces tissue ductility by limiting collagen fibril deformation, and in doing so, reduces the maximum load capacity of the bone.

Keywords

collagen; biomechanics; bone μCT; preclinical studies; metabolism

Introduction

Prevention of fragility fractures, which cause significant morbidity and societal expense, is an important goal for the elderly. The urgency of this goal is increasing with the growing size of the elderly population, and is magnified by the global epidemic of type 2 diabetes (T2D). T2D is an independent risk factor for fracture [1,2], even after accounting for traditional risk factors more prevalent in diabetics, such as neuropathy, decreased visual acuity, and falls [3–6]. Importantly, adults with T2D have a higher fracture risk for a given areal BMD [7] — the main clinical predictor of fracture risk. Identifying the characteristics that make diabetic bone weaker for a given bone mass, which is highly correlated with areal BMD [8], could motivate more accurate diagnostic tools and new therapeutic targets for managing fracture risk in patients with T2D.

Bones derive their resistance to deformation and fracture from physical characteristics that span multiple length scales, and several of these characteristics are independent of bone mass and BMD and could be impaired by T2D. At the nanoscale, collagen fibril stretching and sliding confer ductility to the tissue, which provides resistance to crack initiation and growth [9]. In T2D, hyperglycemia results in several changes to the organic matrix that could impact collagen behavior, including increases in the formation of advanced glycation endproducts (AGEs) that can cross-link the collagen fibrils [10,11]. While AGE accumulation could reduce fibril stretching and sliding and thereby reduce tissue ductility, evidence of this mechanism in a diabetic milieu is limited. In one study, levels of the AGE pentosidine were significantly higher in femora from diabetic WBN/Kob rats, and pentosidine concentration was negatively correlated with whole-bone stiffness and strength [12]. Silva *et al.* reported that elevated pentosidine in ulnae from rats with type 1 diabetes coincided with reduced tissue strength [13]. Compromised tissue behavior has also been reported in humans with T2D [14], although the mechanisms remain unclear.

In addition to altering the physical properties of the collagen, AGE accumulation could reduce bone strength by impairing bone structure, *i.e.,* geometry and microarchitecture.

Optimal bone structure is needed to ensure efficient distribution of mechanical stresses, which influence the propensity for structural failure [15] and thus directly contribute to the maximal force and energy a bone can withstand. In T2D, excessive AGE accumulation could hinder the bone cells' ability to maintain optimal geometry and microarchitecture. For example, AGEs reduce the rate of matrix resorption [16,17]. AGEs can also inhibit the phenotypic expression of osteoblasts [18], interfere with osteoclast differentiation [17], and stimulate secretion of catabolic and pro-inflammatory factors [19]. Accordingly, increased AGE accumulation with diabetes may underlie the impairments in cortical geometry and trabecular microarchitecture that have been reported in rodent models [20–22]. In humans, cortical porosity is significantly higher at the distal radius [23,24] and distal tibia [25] in some cohorts with T2D, including cohorts with a fracture [26]. There is also evidence of thinner cortices at the femoral neck in post-menopausal women with T2D who fracture [27].

To understand how T2D heightens bone fragility, prior studies measured tissue material properties (or AGE concentrations), cortical/trabecular microarchitecture, and whole-bone biomechanical behavior. However, because it was difficult to observe collagen fibril deformations, the basis for any tissue material defects is unclear. Likewise, since the net biomechanical effects of material properties and bone structure on whole-bone strength are intertwined, the relative roles of any deficits in these characteristics resulting from concurrent T2D also remain unknown. This knowledge may be important for accurately assessing fracture risk in T2D and for developing treatment strategies. Here we addressed these issues in a well-characterized and validated rat model of T2D [28]. For the first time, we measured collagen fibril deformation using small angle X-ray scattering (SAXS), and we estimated the relative contributions of tissue material properties and bone structure using micro-CT-based finite element analysis. Using this approach, we sought to test the hypothesis that deficits in tissue material properties in T2D significantly reduce whole-bone strength.

Materials and Methods

Study design

This study was designed with two aims: 1) to evaluate the effects of T2D on tissue material properties; and 2) to measure the contributions of any T2D-induced deficits in tissue material properties on whole-bone biomechanical behavior. To evaluate the effects of T2D, we used a well-established rat model and control animals for the effects of age, disease duration, insulin resistance, obesity, and glycemic control. Developed and validated at the University of California, Davis, the UCD-T2DM rat mimics the pathophysiology of human T2D [28]. Generated by crossing two lines of non-diabetic rats — one with adult-onset obesity and insulin resistance, without defects in either leptin production or leptin receptor signaling (obese Sprague-Dawley, OSD) and one with defective pancreatic beta cell islet function and insulin secretion (ZDF-lean) — the UCD-T2DM rats demonstrate diabetes in both sexes with adult-onset obesity, insulin-resistance, impaired glucose tolerance, and eventual beta cell decompensation. Here we compared the UCD-T2DM rats to two non-diabetic controls: lean Sprague Dawley (LSD) and OSD rats. By comparing the UCD-T2DM rats to OSD rats, which are a genetically similar, obese and insulin-resistant control,

we sought to disentangle the effects of hyperglycemia from the effects of obesity and insulin-resistance, which could independently affect bone behavior [29–31].

We also measured the contribution of tissue material properties to whole-bone behavior. This is difficult to achieve through biomechanical testing alone, so we coupled the tests with high-resolution, micro-CT-based finite element analysis of the same bones. This approach enabled us to simulate a hypothetical scenario: How do bones from diabetic rats behave biomechanically when given the average tissue material properties measured from healthy control rats? By comparing the biomechanical behavior of these hypothetical bones with bones from the diabetic rats having their measured (specimen-specific) material properties, we assessed the unique contribution of tissue material properties. And, by comparing the behavior of the hypothetical bones with bones from healthy rats having identical material properties, we quantified the contributions of bone geometry/microarchitecture — the only remaining variable in the models.

Animals and tissues

Rats were maintained and studied in accordance with Institutional Animal Care and Use Committee-approved protocols at the University of California, Davis (UCD). Ulnae and lumbar fourth (L4) vertebrae were harvested from rats following euthanasia with an overdose of pentobarbital. Six-month-old LSD rats ("control"), OSD rats ("obese") and UCD-T2DM rats (“diabetic”; n = 4–6 rats/group) were studied. The generation and phenotypes of these rats has been previously described [28]. Non-fasted blood glucose was monitored every 2 weeks with a glucose meter to determine the age of diabetes onset (blood glucose concentration >200 mg/dl on two consecutive measurements). As described previously, blood was collected for measurement of circulating glucose, insulin, and HbA1c after an overnight fast at the time of sacrifice [32].

Ulnae and vertebrae were cleaned of soft tissues, and the vertebral posterior elements were embedded in epoxy and mounted in a custom holder of a low-speed diamond blade precision saw. Cranial and caudal endplates were removed while under irrigation to produce vertebral bodies with plano-parallel end surfaces and similar vertebral heights.

Micro-CT

Right ulnae (15-mm-long region) and L4 vertebrae (after endplate removal) were imaged with micro-CT (μCT50; Scanco Medical AG; Brüttisellen, Switzerland) to measure tissue mineralization, bone geometry, and vertebral trabecular microarchitecture (Fig. 1). Bone geometry parameters included ulnar moments of inertia relative to the anterior-posterior and medial-lateral axes at the mid-span (I_{ap} and I_{ml}, respectively) and averaged for entire scan region ($I_{ap\text{-}avg}$ and $I_{ml\text{-}avg}$), cross-sectional area (ulnae; A), and relative mass of the cortical shell (vertebrae; Ct.M [33]). Imaging was performed with a 55 kVp potential, 145 mA current, and 16 μm voxels (ulnae) or 6 μm voxels (vertebrae). Voxel attenuation was converted to mineral density using a 1200 mg HA/cc phantom. Bone mass (bone mineral content, BMC) was the total mineral density for all bone voxels calculated after applying a global threshold to the micro-CT images, and was used as the surrogate for bone quantity in the rats.

Biomechanical testing

After imaging, right ulnae and vertebrae were destructively tested to measure whole-bone biomechanical properties and estimated material properties. Ulnae were loaded to failure in 3-point-bending by placing each bone on two supports (span, L = 15 mm) and applying a laterally directed displacement (d) to the medial aspect of the mid-diaphysis at a rate of 0.01 mm/s. Vertebrae were compressed to failure between platens at a rate of 0.5% strain/sec. All tests were performed on hydrated bones at room temperature using either an electromechanical (ulnae) or servo-hydraulic load frame (vertebrae). Force (F) and displacement data were converted to moments (ulnae, $M = FL/4$) and normalized displacement (ulnae, $d' = 12d/L^2$), and plots of M *vs.* d' (ulnae) or F *vs.* d (vertebrae) were used to calculate whole-bone stiffness, yield force, and ultimate force. We then estimated ulnar tissue material properties (tissue modulus, yield stress and ultimate stress) using the micro-CT-derived geometric parameters and beam theory [13].

Synchrotron small-angle x-ray scattering

Collagen fibril deformation during uniaxial tension testing of the left ulnae was measured using synchrotron small-angle x-ray scattering (SAXS). This approach permits simultaneous, real-time measurement during the tensile test, of the specific strain carried by the collagen fibrils as compared to the bulk tissue strain. The distal and proximal ends of the ulnae were glued to sandpaper strips and secured between clamps. *In situ* tensile tests were performed on hydrated ulnae at a displacement rate of 5 μm/s with a TST350 Tensile Testing Stage (Linkam Scientific Inc.). During testing, the mid-shaft was exposed to X-ray beams of 10 keV energy for 1 s every 7.5 s (450 μm *x* 350 μm beam window). Total radiation was limited to 30 kGy to minimize any effects on mechanical behavior [34]. The collagen d-spacing *i.e.*, regular staggering pattern of the collagen triple helices, was measured from shifts in the Bragg peak positions at increasing amounts of load and converted to collagen fibril strain by normalizing to the d-spacing at zero load. Tissue stress was calculated from cross-sectional area measurements of contralateral ulnae. Detailed explanations on calculation of strain in the collagen fibrils and bone tissue have been previously described [35]. SAXS was performed at beamline 7.3.3 [36] at the Advanced Light Source (Lawrence Berkeley National Laboratory, Berkeley, CA).

Biochemical analysis of AGE accumulation

A fluorimetric assay was used to measure the concentration of AGEs in the left ulnae following *SAXS*. Mid-diaphyseal sections were first decalcified in EDTA and then hydrolyzed in 6N HCl (24 hrs, 110°C). Fluorescence readings of the neutralized lysates (excitation 370 nm, emission 440 nm) were referenced to a quinine sulfate standard [37] and then normalized to the collagen content, which was calculated from the amount of hydroxyproline [38].

Finite element modeling

To study the relative contributions of T2D-induced differences in tissue material properties *vs.* bone geometry and microarchitecture, we performed finite element modeling for the ulnae and vertebrae that had been destructively tested. Finite element models were

constructed from each micro-CT scan using 16 μm-sided (ulnae) or 6 μm-sided (vertebrae) cube-shaped elements. We considered two cases of tissue material properties. In the first case, we assigned each element of the bones from the UCD-T2DM rats a Young's modulus that was based on its voxel-specific tissue mineral density using a previously published power-law relationship [39]. In the second case, we assigned each element the mean Young's modulus that was determined for all elements in the models belonging to the bones from lean Sprague Dawley controls from the same anatomic site. A Poisson's ratio of 0.3 was used in both cases.

High-resolution, linearly elastic finite element analysis was used to determine whole-bone stiffness (vertebrae) or rigidity (ulnae). For the ulnae, we simulated 3-point bending by applying a laterally directed displacement to the nodes at the medial aspect of the mid-diaphysis while constraining the nodes at the lateral aspect of the distal and proximal ends in the medial-lateral direction. Uniaxial compression was applied to the vertebrae, with the nodes along the cranial and caudal surfaces free to move in-plane.

We also performed geometrically and materially nonlinear analysis using the tissue properties measured from the SAXS experiments. Here, bone tissue was modeled using a rate-independent elasto-plasticity model [40] and homogeneous isotropic tissue material properties: animal-specific Young's modulus and tensile yield strain measured by SAXS, Poisson's ratio of 0.3, and a compressive yield strain of 0.69% [41]. For the hypothetical case, bones from UCD-T2DM rats were assigned the mean Young's modulus and mean tensile yield strain that was measured for the control bones by SAXS. Owing to the large size of the models (up to 87 million elements each), nonlinear finite element analysis was carried out for a subset of ulnae and vertebrae. Simulations were performed at the Texas Advanced Computing Center using an implicit, parallel finite element code [42].

Outcomes and statistics

To test our hypothesis that diabetes coincides with deficits in tissue material properties and bone structure, we used ANOVA with Tukey-Kramer post-hoc tests to determine group differences. Despite the small sample size per group, parametric tests were used because the data did not violate the normality assumption ($p > 0.05$, Shapiro-Wilk test) or equal variance assumption. We also compared ratios of whole-bone biomechanical properties (stiffness, yield force, ultimate moment, *etc.*) to BMC between groups. This allowed us to compare the biomechanical performance of bones that were different sizes and to determine if diabetes associated with lower whole-bone strength for a given bone mass. Importantly, this approach is analogous to comparing regression models of biomechanical properties *vs.* bone mass, and it yields similar conclusions about the existence of factors beyond bone quantity that may be contributing to differences in whole-bone biomechanical properties [43]. To evaluate the contributions of material property deficits *vs.* structural deficits in T2D, we performed two comparisons. First, unpaired *t*-tests were used to compare finite element-predicted biomechanical properties between bones from LSD and UCD-T2DM rats that were assigned the same material properties (effects of bone structure only). Next, paired *t*-tests were used to compare predictions between the bones from the UCD-T2DM rats with and without specimen-specific material properties (effects of material properties only). Statistical tests

were performed with JMP 12 Pro (SAS Institute; Cary, NC). Significance is defined by $p < 0.05$. Data are given as mean ± SEM.

Results

Blood glucose levels indicated that the UCD-T2DM rats were diabetic for 69 ± 7 days (range: 46–89 days) at the time of sacrifice. Body weights, blood glucose, and HbA1c for these same rats were reported previously [32]. Of note, obese OSD rats and those with diabetes had significantly higher body weights than age-matched lean LSD controls. Whereas both OSD and UCD-T2DM rats had over two-fold higher insulin levels (1.4 ± 0.3 ng/ml) indicative of insulin resistance compared with lean LSD controls (0.6 ± 0.07 ng/ml), only the UCD-T2DM rats were hyperglycemic (HbA1c 11.8 ± 1.28% *vs.* 4.5 ± 0.09% and 4.3 ± 0.06% in LSD and OSD rats, respectively, $p < 0.0001$).

T2D and obesity reduce whole-bone biomechanical properties for a given bone mass

At the whole-bone level, obese rats and those with diabetes had significantly reduced whole-bone biomechanical properties per unit bone mass. Overall, obese rats had improved vertebral stiffness, yield force, and ultimate force, while diabetic UCD-T2DM rats generally had inferior properties (Table 1). However, both obese rats and those with diabetes had significantly higher BMC (Table 2), and the biomechanical properties were highly correlated with BMC ($r^2 = 0.49–0.76$, $p < 0.005$). To identify whether factors beyond BMC may have contributed to differences in whole-bone biomechanical properties, we compared ratios of whole-bone stiffness- and strength-to-BMC between groups [43]. After normalizing the properties by BMC, the OSD and UCD-T2DM rats had 47% and 22% lower vertebral stiffness ($p < 0.01$; Fig. 2A), 23% lower yield force ($p < 0.005$, Fig. 2B), and 27% lower ultimate force ($p < 0.001$; Fig. 2C). Similarly, per unit BMC, the ulnae from OSD and UCD-T2DM rats had 17–26% lower rigidity ($p < 0.001$; Fig. 2D), 22–32% lower yield moment ($p < 0.05$; Fig. 2E) and 22% lower ultimate moment ($p < 0.01$; Fig. 2F).

T2D and obesity compromise vertebral geometry and microarchitecture

The reduced whole-bone stiffness and strength measured for a given bone mass coincided with significant deficits in vertebral geometry and trabecular microarchitecture (Table 2). Compared to lean controls, vertebrae from diabetic rats demonstrated 33% lower bone volume fraction (BV/TV, $p < 0.001$) and trabeculae that were 14% thinner (Tb.Th, $p < 0.01$) and more rod-like (SMI, $p < 0.01$). In the OSD rats, the higher bone mass reflected a larger trabecular compartment, as the relative mass of the cortical bone was 15% lower (Ct.M, $p < 0.001$ *vs.* lean control).

In the ulnae, both OSD and UCD-T2DM rats had 15–20% greater bone mass ($p < 0.005$). However, the additional bone mass in these groups mainly benefited resistance to anterior-posterior bending (higher I_{ml}; Table 2), which provides minimal resistance to medial-lateral bending despite the larger cross-sectional area. Section modulus and moment of inertia relative to the anterior-posterior axis (I_{ap}) were similar in all groups. This suggests that the T2D-related reductions in ulnar rigidity/BMC, yield moment/BMC, and ultimate moment/BMC are mainly attributable to deficits in tissue material behavior.

T2D impairs tissue material properties and reduces collagen fibril ultimate strain

In the UCD-T2DM rats with hyperglycemia, the observed impairments in whole-bone biomechanical properties for a given bone mass were attributable to substantial deficits in tissue material properties. We first used beam theory to estimate the tissue material properties from the bending tests (Table 3). Results indicated that diabetes but not obesity reduced the tissue modulus by 16% ($p < 0.05$), the tissue yield strength by 28% ($p < 0.01$), and the tissue ultimate strength by 12% ($p < 0.05$). To complement these results, the contralateral ulnae from the lean LSD rats and UCD-T2DM rats were loaded in uniaxial tension (Table 3). Tensile measurements corroborated the diabetes-induced reduction in tissue modulus and further revealed that diabetes reduced the uniaxial tissue yield strain by 24% ($p < 0.005$) and ultimate strain, or ductility, by 31% ($p < 0.05$).

To gain insight into the deficits in tissue material properties observed in UCD-T2DM rats, we used SAXS to measure the specific strain in the collagen fibrils associated with their deformation during uniaxial tensile testing. Below 0.5% tissue strain, there was no significant difference between collagen fibril strain in the bones from diabetic rats and lean controls (Fig. 3A). However, above 0.5% tissue strain, diabetes reduced fibril strain by nearly a half. At the ultimate tissue strain, diabetes reduced the ultimate fibril strain by 40% ($p < 0.05$; Fig. 3B).

Diabetes increases AGE concentrations in bone

As expected from our previous study [32], hyperglycemia significantly increased AGE levels. In the rats with diabetes, AGE concentrations in the ulna mid-diaphyses were 27% higher compared with lean LSD control rats (0.37 ± 0.013 *vs.* 0.29 ± 0.014 ng quinine fluorescence/μg collagen; $p < 0.05$). AGE levels in the ulnae from obese rats without diabetes (0.33 ± 0.013 ng quinine fluorescence/μg collagen) were not statistically different from lean controls ($p = 0.30$).

Relative contributions of tissue material properties vs. bone geometry and microarchitecture

The impairments in whole-bone stiffness and strength per unit bone mass caused by diabetes were attributable to deficits in vertebral geometry and trabecular microarchitecture and to deficits in tissue material properties. To estimate their relative contributions, we compared high-resolution finite element models of the bones from UCD-T2DM rats with and without specimen-specific material properties to models of the bones from lean controls. For the vertebrae, including the diminished material properties (specimen-specific tissue modulus and yield strain) caused by diabetes significantly reduced stiffness by 7% (Fig. 4A, $p < 0.01$) and yield force by 17.4% (Fig. 4B, $p < 0.0001$), whereas modeling only the deficits in vertebral geometry and trabecular microarchitecture significantly reduced yield force by 18% (Fig. 4B, $p < 0.05$). For the ulnae, including the diminished material properties caused by diabetes reduced rigidity by 4.7% (Fig. 4C, $p = 0.07$) and yield moment by 19.9% (Fig. 4D, $p < 0.01$), whereas the differences in ulnar geometry had a small, non-significant effect on rigidity and yield moment.

Discussion

These results demonstrate that T2D significantly reduces whole-bone stiffness and strength for a given bone mass. This was attributable to two factors. First, diabetes was associated with deficits in bone geometry and trabecular microarchitecture (Table 2). For the vertebrae, this included thinner and more rod-like trabeculae, which are more prone to bending deformations that require only a small amount of tissue failure [15]. For the ulnae, this included inefficient distribution of bone mass; diabetes led to a greater amount of bone matrix at the anterior and posterior aspects of the diaphysis, which provides minimal resistance to medial-lateral bending despite the increase in overall bone mass. Second, the lower whole-bone stiffness and strength for a given bone mass that associated with diabetes was attributable to substantial deficits in tissue material properties (Table 3). Tissue ductility is conferred primarily by collagen fibril deformation. Our data show for the first time that T2D significantly impairs collagen fibril deformation, *i.e.*, that the collagen in T2D-affected bone cannot carry as much strain, and that these nanoscale changes in collagen behavior coincide with deficits in the elastic, yield, and ultimate properties of the bone tissue. Importantly, the net biomechanical effects of these material property deficits were substantial. Prescribing T2D-specific tissue yield strains in high-resolution finite element models reduced vertebral strength by 17.4%, a similar amount as the structural deficits (18%). For the ulnae, the effects of material property deficits on bone strength were 3.4-fold greater than the structural deficits (19.9% *vs.* 5.8%). Taken together, these findings provide new insight into the factors that increase bone fragility for a given bone mass in T2D; not only does T2D associate with alterations to bone geometry/microarchitecture that make the structure less biomechanically efficient, but T2D also reduces tissue ductility by impairing collagen fibril deformation, and in doing so, reduces the maximum load capacity of the bone.

A novel finding of this study is that diabetes significantly reduced collagen fibril deformation. In healthy bone, collagen fibril deformation such as stretching and sliding is a primary intrinsic toughening mechanism that confers ductility to the tissue [35,44,45]. Fibril stretching is believed to predominate at smaller applied strains, while fibril sliding is thought to predominate at larger applied strains and contribute to the tissue's ability to deform plastically [44]. Here, diabetes reduced fibril strain for a given tissue strain at larger applied strains (>0.5%; Fig. 3A) — implying that the fibrils have become stiffer with diabetes — and there was a 40% reduction in ultimate fibril strain (Fig. 3B). Without this form of energy dissipation at the mineralized fibril scale, there is less resistance to microcrack initiation and propagation, and there is degradation in the ductility and intrinsic toughness of the bone [44]. Thus, we believe that reduced collagen fibril deformation due to impaired fibril sliding explains why the bones from diabetic rats exhibited a 24% lower tissue yield strain and 31% lower tissue ductility compared to the bones from lean controls. These deficits in collagen behavior and tissue ductility with diabetes reduce the load capacity of the bone, and they coincided with 27% higher concentrations of non-enzymatic cross-links (AGEs). Results from previous studies indicate that AGE accumulation with ageing reduces collagen fibril deformation [44] and that diabetes accelerates AGE accumulation [10]. Our current results extend those prior findings by demonstrating that increased AGE accumulation with diabetes

associates with reduced collagen deformation, and that the corresponding reduction in tissue yield strain accounts for a large proportion of the overall loss in whole-bone strength.

Our results showed that T2D associates with weaker ulnae and vertebrae than would be predicted based on bone mass alone. Fracture risk assessment is based on areal BMD by DXA—a measure of bone quantity that is highly correlated with DXA-derived bone mass [8]. Yet, adults with T2D have a higher fracture risk than would be predicted based on their bone quantity [7]. Here, weaker bone strength for a given bone mass in diabetes was attributable to deficits in tissue material properties and bone structure. Although requiring confirmation in humans, our findings suggest that knowledge about both tissue material properties and bone structure may improve fracture risk assessment in T2D. Clinical methodologies for measuring material properties and bone structure in patients with T2D using reference point indentation [14] and high-resolution peripheral quantitative computed tomography [25,26] are promising, but these methodologies are not widespread and prospective studies are needed. Related, our findings also suggest that anti-fracture treatments may need to improve both tissue material properties and structure to fully restore bone strength in a diabetic milieu. Little is known about the effects of anti-fracture treatment in subjects with T2D [46]. The effects of glycemic control on AGEs in bone are also unclear; reducing any excessive intake of dietary AGEs may be important too [47].

Another notable finding is that insulin resistance and hyperglycemia had distinct effects on bone structure and material properties. Both obese insulin-resistant OSD rats and UCD-T2DM rats with hyperglycemia had lower whole-bone biomechanical properties per unit bone mass; however, only the rats with hyperglycemia had significant impairments in tissue material properties. While OSD rats had 2.5% lower vertebral TMD and 3.1% lower ulnar TMD, assigning specimen-specific tissue material properties based on TMD in high-resolution finite element models of the OSD rats' bones reduced vertebral stiffness and ulna rigidity by just 2.8% and 2.2%, respectively (data not shown). In combination with the similar tissue material properties derived from the bending tests of OSD and LSD ulnae, these findings suggest that the lower whole-bone biomechanical properties per unit bone mass in the obese, normoglycemic rats is attributable mainly to structural deficiencies. For the vertebra, we believe this is mainly arises due to the lower percentage of cortical bone, which has a greater load-bearing role [39]. For the ulna, we believe this mainly reflects the inefficient distribution of bone mass. Moreover, bone mass was significantly higher at both sites. This is consistent with evidence from human studies that report more trabecular and cortical bone at the distal radius and tibia in obese individuals [48,49]; however, additional research is needed to clarify whether differences in the distribution of bone mass explain the association between obesity and higher fracture risk for a given bone quantity [50].

This study had several limitations. Most importantly, we did not study animals with an advanced duration and severity of diabetes, which may limit the generality of the conclusions. However, since reductions in collagen deformation coincided with AGE accumulation, and because AGEs increase with diabetes duration and severity [12,22], bone biomechanical behavior would both be expected to progressively worsen with a longer duration of diabetes and greater degree of hyperglycemia. This is consistent with findings in bones from Zucker Diabetic Sprague Dawley (ZDSD) rats, where AGEs and biomechanical

impairments increased with disease duration [12]. A second limitation is that we used a non-diabetic control rat that is not a littermate or the same strain. Thus, we did not account for any potential strain-related differences that might have contributed to the observed bone phenotype. However, we believe the bone phenotype in the UCD-T2DM rats mainly reflects the effects of diabetes, and future studies are needed to evaluate the impact of any strain-related differences. It is also worth noting that we focused on the ulna because its length-to-width ratio makes it suitable for estimating tissue material properties from beam theory equations. Although the ulna is not a primary fracture site in humans, our results from the ulnar mid-diaphysis should be representative of long-bone behavior in general. A technical limitation is that the assumed constitutive model used in the nonlinear finite element analyses incorporated only the elastic and yield behavior of the bone tissue, and thus our simulations did not include post-yield behavior or fracture. Since individual trabeculae rarely fracture before the yield point of the structure [51,52], we expect that our finite element-derived conclusions about whole-bone biomechanical properties at yield are valid despite this limitation. Finally, our simulations assumed that diabetes had similar effects on the material properties of cortical and trabecular bone, and this remains to be confirmed. Results from a glycation study indicate that trabecular bone may accumulate more AGEs than cortical bone [53], which suggests that the estimated contribution of material property deficits to whole-vertebral behavior is conservative.

In summary, these findings showed that in addition to causing alterations to the bone structure that make it less biomechanically efficient for a given bone mass, T2D reduces tissue ductility by impairing collagen fibril deformation, and in doing so, reduces the maximum load capacity of the bone. The diminished tissue material properties were specific to the rats with hyperglycemia and coincided with high concentrations of AGEs. Taken together, these results provide mechanistic insight into the structural and material contributors to diabetic bone fragility, and suggest that both bone structure and material properties may be important targets to more accurately assess fracture risk in T2D and to develop treatment strategies.

Acknowledgements

This study received support from the Swiss National Science Foundation (CA: P300P2_167583), National Institutes of Health (PJH: DK095980; HL107256; HL121324; TNA: DE019284; AJF: AR070198 and AR066262), National Science Foundation via XSEDE (AJF: TG-BCS120005), and Department of Defense (TNA: OR130191). Dr. Havel's laboratory also received research support from a Multi-campus grant (UC, Davis, UC, Berkeley, and UC, San Francisco) from the University of California Office of the President. Beamline 7.3.3 of the Advanced Light Source is supported by the Director of the Office of Science, Office of Basic Energy Sciences, of the U.S. Department of Energy under Contract No. DE-AC02–05CH11231. We thank Alfred Li, Roberto Ixta, and Sara Sampson for their assistance with imaging and experiments, and also the A.Z. Weber group for providing their tensile stage, which was supported by DOE EERE Fuel-Cell Performance and Durability Consortium (FC-PAD).

References

1. Fan Y, Wei F, Lang Y, Liu Y. Diabetes mellitus and risk of hip fractures: a meta-analysis Osteoporos Int. Jan; 2016 27(1):219. [PubMed: 26264604]
2. Janghorbani M, Feskanich D, Willett WC, Hu F. Prospective study of diabetes and risk of hip fracture: the Nurses' Health Study Diabetes Care. Jul; 2006 29(7):1573. [PubMed: 16801581]

3. Bonds DE, Larson JC, Schwartz AV, Strotmeyer ES, Robbins J, Rodriguez BL. Risk of fracture in women with type 2 diabetes: the Women's Health Initiative Observational Study J Clin Endocrinol Metab. Sep; 2006 91(9):3404. [PubMed: 16804043]
4. Strotmeyer ES, Cauley JA, Schwartz AV, Nevitt MC, Resnick HE, Bauer DC. Nontraumatic fracture risk with diabetes mellitus and impaired fasting glucose in older white and black adults: the health, aging, and body composition study Arch Intern Med. Jul 25; 2005 165(14):1612. [PubMed: 16043679]
5. Schwartz AV, Sellmeyer DE, Ensrud KE, Cauley JA, Tabor HK, Schreiner PJ. Older women with diabetes have an increased risk of fracture: a prospective study J Clin Endocrinol Metab. Jan; 2001 86(1):32. [PubMed: 11231974]
6. de L II, van der Klift M, de Laet CE, van Daele PL, Hofman A, Pols HA. Bone mineral density and fracture risk in type-2 diabetes mellitus: the Rotterdam Study Osteoporos Int. Dec; 2005 16(12): 1713. [PubMed: 15940395]
7. Schwartz AV, Vittinghoff E, Bauer DC, Hillier TA, Strotmeyer ES, Ensrud KE. Association of BMD and FRAX score with risk of fracture in older adults with type 2 diabetes Jama-J Am Med Assoc. Jun 1; 2011 305(21):2184.
8. Deng HW, Xu FH, Davies KM, Heaney R, Recker RR. Differences in bone mineral density, bone mineral content, and bone areal size in fracturing and non-fracturing women, and their interrelationships at the spine and hip J Bone Miner Metab. 2002; 20(6):358. [PubMed: 12434164]
9. Launey ME, Buehler MJ, Ritchie RO. On the Mechanistic Origins of Toughness in Bone Annual Review of Materials Research. 2010; 40(1):25.
10. Karim L, Bouxsein ML. Effect of type 2 diabetes-related non-enzymatic glycation on bone biomechanical properties Bone. Jan.2016 82:21. [PubMed: 26211993]
11. Yamamoto M, Sugimoto T. Advanced Glycation End Products, Diabetes, and Bone Strength Curr Osteoporos Rep. Dec; 2016 14(6):320. [PubMed: 27704396]
12. Saito M, Fujii K, Mori Y, Marumo K. Role of collagen enzymatic and glycation induced cross-links as a determinant of bone quality in spontaneously diabetic WBN/Kob rats Osteoporos Int. Oct; 2006 17(10):1514. [PubMed: 16770520]
13. Silva MJ, Brodt MD, Lynch MA, McKenzie JA, Tanouye KM, Nyman JS. Type 1 diabetes in young rats leads to progressive trabecular bone loss, cessation of cortical bone growth, and diminished whole bone strength and fatigue life J Bone Miner Res. Sep; 2009 24(9):1618. [PubMed: 19338453]
14. Farr JN, Drake MT, Amin S, Melton LJ 3rd, McCready LK, Khosla S. In Vivo assessment of bone quality in postmenopausal women with type 2 diabetes J Bone Miner Res. Oct 1.2013
15. Fields AJ, Nawathe S, Eswaran SK, Jekir MG, Adams MF, Papadopoulos P. Vertebral fragility and structural redundancy J Bone Miner Res. May 23; 2012 27(10):2152. [PubMed: 22623120]
16. Ural A, Janeiro C, Karim L, Diab T, Vashishth D. Association between non-enzymatic glycation, resorption, and microdamage in human tibial cortices Osteoporos Int. Mar; 2015 26(3):865. [PubMed: 25326375]
17. Valcourt U, Merle B, Gineyts E, Viguet-Carrin S, Delmas PD, Garnero P. Non-enzymatic glycation of bone collagen modifies osteoclastic activity and differentiation J Biol Chem. Feb 23; 2007 282(8):5691. [PubMed: 17142454]
18. Katayama Y, Akatsu T, Yamamoto M, Kugai N, Nagata N. Role of nonenzymatic glycosylation of type I collagen in diabetic osteopenia J Bone Miner Res. 1996; 11(7):931. [PubMed: 8797113]
19. Takagi M, Kasayama S, Yamamoto T, Motomura T, Hashimoto K, Yamamoto H. Advanced glycation endproducts stimulate interleukin-6 production by human bone-derived cells J Bone Miner Res. 1997; 12(3):439. [PubMed: 9076587]
20. Prisby RD, Swift JM, Bloomfield SA, Hogan HA, Delp MD. Altered bone mass, geometry and mechanical properties during the development and progression of type 2 diabetes in the Zucker diabetic fatty rat J Endocrinol. Dec; 2008 199(3):379. [PubMed: 18755885]
21. Reinwald S, Peterson RG, Allen MR, Burr DB. Skeletal changes associated with the onset of type 2 diabetes in the ZDF and ZDSD rodent models Am J Physiol Endocrinol Metab. Apr; 2009 296(4):E765. [PubMed: 19158319]

22. Creecy A, Uppuganti S, Merkel AR, O'Neal D, Makowski AJ, Granke M. Changes in the Fracture Resistance of Bone with the Progression of Type 2 Diabetes in the ZDSD Rat Calcif Tissue Int. Sep; 2016 99(3):289. [PubMed: 27209312]
23. Burghardt AJ, Issever AS, Schwartz AV, Davis KA, Masharani U, Majumdar S. High-resolution peripheral quantitative computed tomographic imaging of cortical and trabecular bone microarchitecture in patients with type 2 diabetes mellitus J Clin Endocrinol Metab. Nov; 2010 95(11):5045. [PubMed: 20719835]
24. Yu EW, Putman MS, Derrico N, Abrishamanian-Garcia G, Finkelstein JS, Bouxsein ML. Defects in cortical microarchitecture among African-American women with type 2 diabetes Osteoporos Int. Feb; 2015 26(2):673. [PubMed: 25398431]
25. Samelson EJ, Demissie S, Cupples LA, Zhang X, Xu H, Liu CT. Diabetes and Deficits in Cortical Bone Density, Microarchitecture, and Bone Size: Framingham HR-pQCT Study J Bone Miner Res. Sep 20.2017
26. Patsch JM, Burghardt AJ, Yap SP, Baum T, Schwartz AV, Joseph GB. Increased cortical porosity in type 2 diabetic postmenopausal women with fragility fractures J Bone Miner Res. Feb; 2013 28(2):313. [PubMed: 22991256]
27. Heilmeier U, Carpenter DR, Patsch JM, Harnish R, Joseph GB, Burghardt AJ. Volumetric femoral BMD, bone geometry, and serum sclerostin levels differ between type 2 diabetic postmenopausal women with and without fragility fractures Osteoporos Int. Apr; 2015 26(4):1283. [PubMed: 25582311]
28. Cummings BP, Digitale EK, Stanhope KL, Graham JL, Baskin DG, Reed BJ. Development and characterization of a novel rat model of type 2 diabetes mellitus: the UC Davis type 2 diabetes mellitus UCD-T2DM rat Am J Physiol Regul Integr Comp Physiol. Dec; 2008 295(6):R1782. [PubMed: 18832086]
29. Shanbhogue VV, Mitchell DM, Rosen CJ, Bouxsein ML. Type 2 diabetes and the skeleton: new insights into sweet bones Lancet Diabetes Endocrinol. Feb; 2016 4(2):159. [PubMed: 26365605]
30. Srikanthan P, Crandall CJ, Miller-Martinez D, Seeman TE, Greendale GA, Binkley N. Insulin resistance and bone strength: findings from the study of midlife in the United States J Bone Miner Res. Apr; 2014 29(4):796. [PubMed: 23983216]
31. Ionova-Martin SS, Do SH, Barth HD, Szadkowska M, Porter AE, Ager JW 3rd. Reduced size-independent mechanical properties of cortical bone in high-fat diet-induced obesity Bone. Jan; 2010 46(1):217. [PubMed: 19853069]
32. Fields AJ, Johansen BB, Metz LN, Miller S, La B, Liebenberg EC. Alterations in intervertebral disc composition, matrix homeostasis and biomechanical behavior in the UCD-T2DM rat model of type 2 diabetes J Orthop Res. Jan 29.2015
33. Fields AJ, Eswaran SK, Jekir MG, Keaveny TM. Role of trabecular microarchitecture in whole-verterbal body biomechanical behavior J Bone Miner Res. 2009; 29(9):1523.
34. Barth HD, Zimmermann EA, Schaible E, Tang SY, Alliston T, Ritchie RO. Characterization of the effects of x-ray irradiation on the hierarchical structure and mechanical properties of human cortical bone Biomaterials. Dec 2011; 32(34):8892. [PubMed: 21885114]
35. Acevedo C, Bale H, Gludovatz B, Wat A, Tang SY, Wang M. Alendronate treatment alters bone tissues at multiple structural levels in healthy canine cortical bone Bone. Dec.2015 81:352. [PubMed: 26253333]
36. Hexemer A, Bras W, Glossinger J, Schaible E, Gann E, Kirian R. A SAXS/WAXS/GISAXS Beamline with Multilayer Monochromator J Phys Conf Ser. 2010; 247
37. Advanced glycation end-products and bone fractures. IBMS BoneKEy: International Bone and Mineral Society; 2009. p. 268-78.
38. Woessner JF Jr.. The determination of hydroxyproline in tissue and protein samples containing small proportions of this imino acid Arch Biochem Biophys. May.1961 93:440. [PubMed: 13786180]
39. Easley SK, Jekir MG, Burghardt AJ, Li M, Keaveny TM. Contribution of the intra-specimen variations in tissue mineralization to PTH- and raloxifene-induced changes in stiffness of rat vertebrae Bone. Apr; 2010 46(4):1162. [PubMed: 20034599]

40. Papadopoulos P, Lu J. A general framework for the numerical solution of problems in finite elasto-plasticity Comput Methods Appl Mech Eng. 1998; 159(1–2):1.
41. Bevill G, Farhamand F, Keaveny TM. Heterogeneity of yield strain in low-density versus high-density human trabecular bone J Biomech. Sep 18; 2009 42(13):2165. [PubMed: 19700162]
42. AdamsMF, BayraktarHH, KeavenyTM, PapadopoulosP. Ultrascalable implicit finite element analyses in solid mechanics with over a half a billion degrees of freedom. ACM/IEEE Proceedings of SC2004: High Performance Networking and Computing2004.
43. Hernandez CJ, Keaveny TM. A biomechanical perspective on bone quality Bone. Dec; 2006 39(6): 1173. [PubMed: 16876493]
44. Zimmermann EA, Schaible E, Bale H, Barth HD, Tang SY, Reichert P. Age-related changes in the plasticity and toughness of human cortical bone at multiple length scales Proc Natl Acad Sci U S A. Aug 30; 2011 108(35):14416. [PubMed: 21873221]
45. Carriero A, Zimmermann EA, Paluszny A, Tang SY, Bale H, Busse B. How tough is brittle bone? Investigating osteogenesis imperfecta in mouse bone J Bone Miner Res. Jun; 2014 29(6):1392. [PubMed: 24420672]
46. Napoli N, Chandran M, Pierroz DD, Abrahamsen B, Schwartz AV, Ferrari SL. Mechanisms of diabetes mellitus-induced bone fragility Nat Rev Endocrinol. Apr; 2017 13(4):208. [PubMed: 27658727]
47. Illien-Jünger S, Palacio-Mancheno P, Kindschuh WF, Chen X, Sroga GE, Vashishth D. Dietary Advanced Glycation End Products Have Sex- and Age-Dependent Effects on Vertebral Bone Microstructure and Mechanical Function in Mice J Bone Miner Res. n/a-n/a.
48. Sornay-Rendu E, Boutroy S, Vilayphiou N, Claustrat B, Chapurlat RD. In obese postmenopausal women, bone microarchitecture and strength are not commensurate to greater body weight: the Os des Femmes de Lyon (OFELY) study J Bone Miner Res. Jul; 2013 28(7):1679. [PubMed: 23371055]
49. Andersen S, Frederiksen KD, Hansen S, Brixen K, Gram J, Stoving RK. Bone structure and estimated bone strength in obese patients evaluated by high-resolution peripheral quantitative computed tomography Calcif Tissue Int. Jul; 2014 95(1):19. [PubMed: 24736885]
50. Johansson H, Kanis JA, Oden A, McCloskey E, Chapurlat RD, Christiansen C. A meta-analysis of the association of fracture risk and body mass index in women J Bone Miner Res. Jan; 2014 29(1): 223. [PubMed: 23775829]
51. Fyhrie DP, Schaffler MB. Failure mechanisms in human vertebral cancellous bone Bone. 1994; 15(1):105. [PubMed: 8024844]
52. Wachtel EF, Keaveny TM. Dependence of trabecular damage on mechanical strain J Orthop Res. 1997; 15:781. [PubMed: 9420610]
53. Karim L, Tang SY, Sroga GE, Vashishth D. Differences in non-enzymatic glycation and collagen cross-links between human cortical and cancellous bone Osteoporos Int. Sep; 2013 24(9):2441. [PubMed: 23471564]

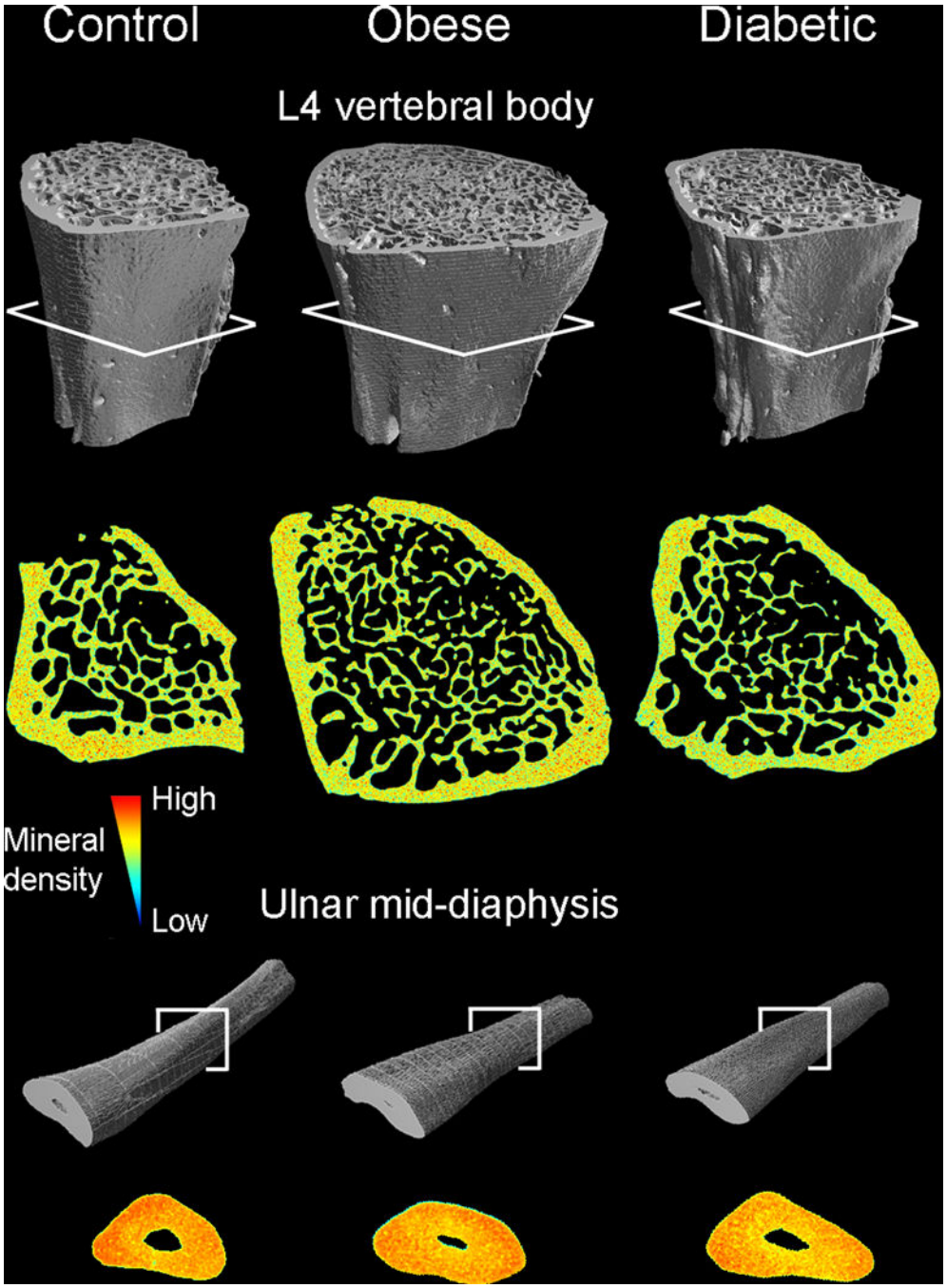

Figure 1.

L4 vertebrae (without endplates) and right ulnae (15-mm long region from the mid-shaft) from lean control rats, obese non-diabetic rats, and diabetic obese rats. Bones were scanned with micro-CT prior to mechanical testing, and the scans were then used to create high-resolution finite element models. Mineral density-shaded cross-sections from obese rats and those with diabetes illustrate differences in bone geometry and trabecular microarchitecture compared to those from lean controls.

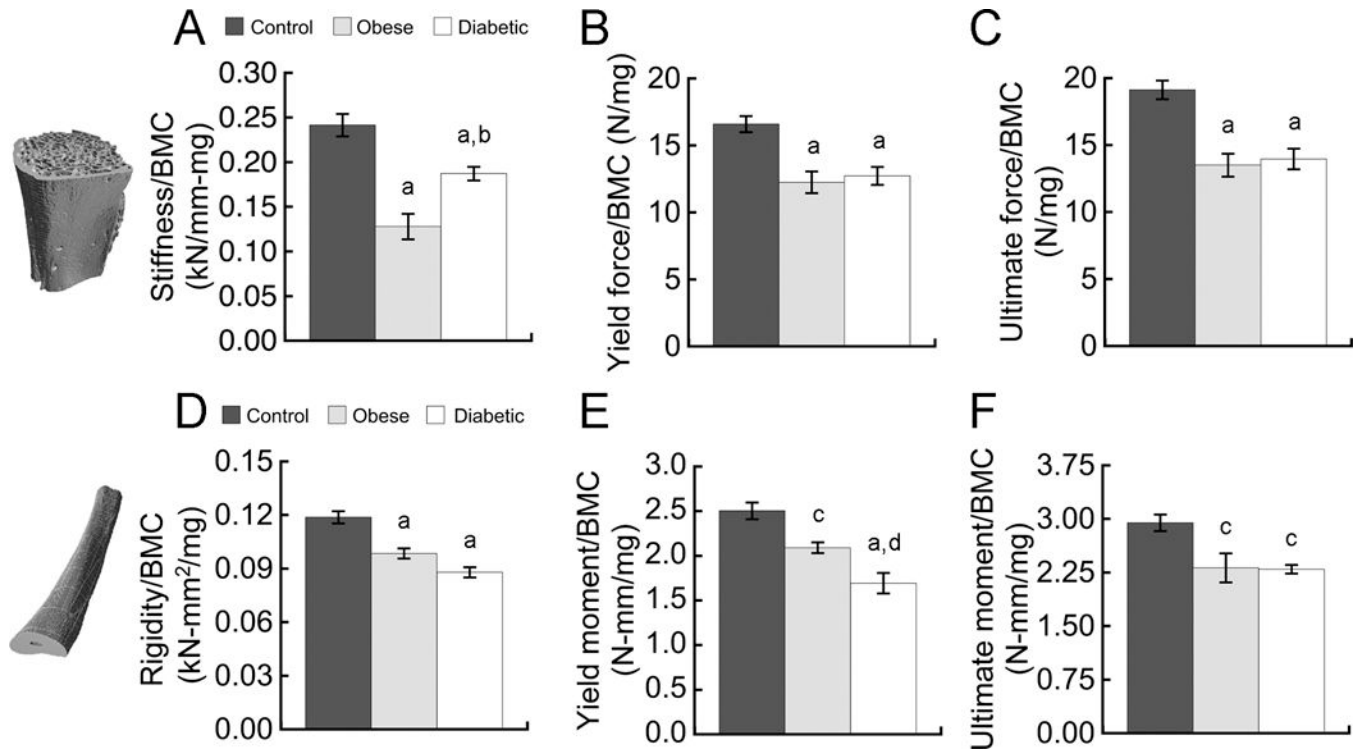

Figure 2.

Obese rats and those with diabetes showed significant reductions in whole-bone biomechanical properties per unit bone mass, BMC. Vertebral properties (A-C) were measured in compression; unlar mid-shaft properties (D-F) were measured in 3-point bending. Data are mean ± SEM for $n = 5–6$ rats/group. [a] $p < 0.01$ vs. control; [b] $p < 0.01$ vs. obese; [c] $p < 0.05$ vs. control; [d] $p < 0.05$ vs. obese

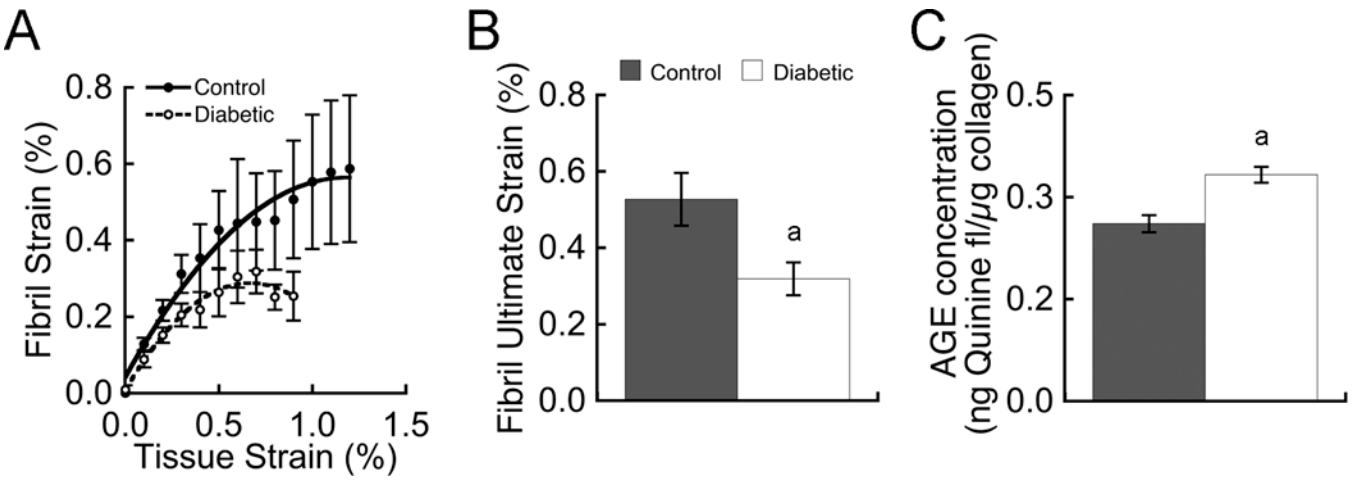

Figure 3.

Collagen fibril deformation during ulna tensile testing was measured by SAXS. Diabetes reduced fibril strain, particularly at tissue strains above 0.5% (A) and culminating with a 40% reduction in fibril ultimate strain (B). Reductions in fibril strain coincided with a 27% increase in AGEs (C). Data are mean ± SEM for $n = 4–5$ rats/group. [a] $p < 0.05$ vs. control

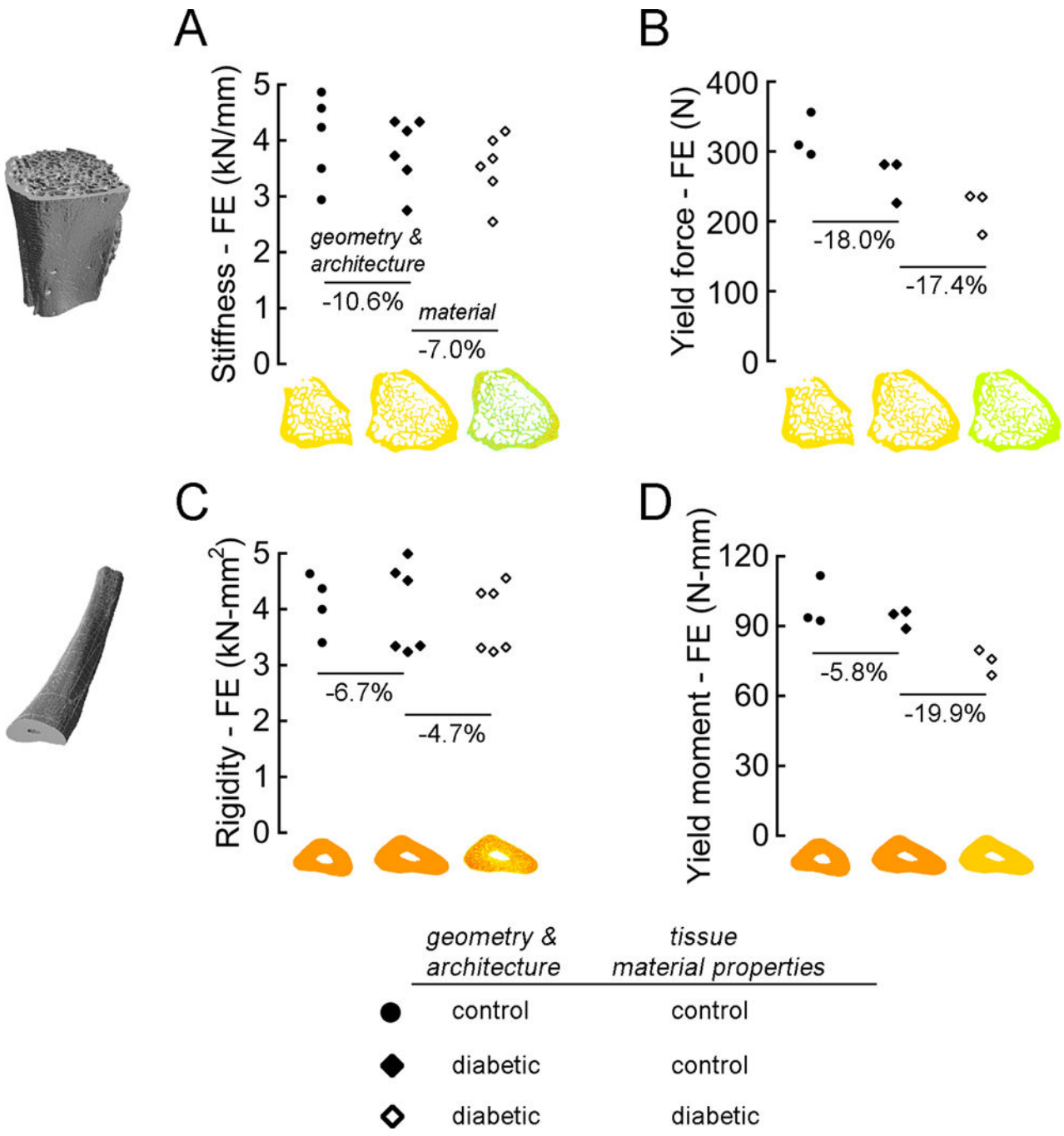

Figure 4.

High-resolution finite element analysis of the vertebrae (A & B) and ulnae (C & D) was used to estimate the relative roles of diabetes-induced deficits in bone geometry and architecture *vs.* material properties. Vertebral behavior was evaluated in compression; unlar mid-shaft behavior was evaluated in 3-point bending. For the elastic biomechanical properties (A & C), models of the bones from lean control rats and those with diabetes were assigned either the average tissue modulus of the bones in the control group or the specimen-specific tissue modulus derived from the micro-CT-based measurements of tissue

mineral density. For the biomechanical properties at yield (B & D), models of the bones were assigned either the average tissue modulus and tissue yield strain of the bones in the control group or the specimen-specific tissue modulus and yield strain measured from the SAXS experiments.

Table 1

Biomechanical properties of vertebrae and ulnae determined by uniaxial compression and 3-point bending (mean ± SEM).

	Lean (*n* = 6 rats)	Obese (*n* = 6 rats)	Diabetic (*n* = 6 rats)	ANOVA *p*-value
Vertebra (compression)				
Stiffness (kN/mm)	4.16 ± 0.21	4.84 ± 0.15	3.53 ± 0.16[a,b]	< 0.001
Yield force (N)	290 ± 24	439 ± 23[a]	243 ± 20[b]	< 0.001
Ultimate force (N)	335 ± 29	483 ± 18[a]	267 ± 23[b]	< 0.001
Ulna (bending)				
Rigidity (kN-mm^2)	4.49 ± 0.21	4.51 ± 0.14	3.83 ± 0.17[a,b]	0.024
Yield moment (N-mm)	96.6 ± 6.0	95.8 ± 3.3	74.4 ± 7.2[a,b]	0.022
Ultimate moment (N-mm)	110.9 ± 6.4	106.1 ± 3.0	100.2 ± 6.7	0.420

[a] $p < 0.05$ *vs.* control by posthoc test

[b] $p < 0.05$ *vs.* obese by posthoc test

Table 2

Bone mass, geometry, and microarchitecture determined from micro-CT (mean ± SEM).

	Lean (*n* = 5–6 rats)	Obese (*n* = 6 rats)	Diabetic (*n* = 6 rats)	ANOVA *p*-value
Vertebra				
Bone mass, BMC (mg)	17.0 ± 1.7	33.1 ± 2.4[a]	19.1 ± 1.1[b]	< 0.001
BV/TV	0.29 ± 0.01	0.28 ± 0.02	0.20 ± 0.01[a,b]	< 0.001
Tb.N (mm^{-1})	3.4 ± 0.1	3.7 ± 0.2	3.0 ± 0.1[b]	0.009
Tb.Th (mm)	0.084 ± 0.001	0.080 ± 0.002	0.073 ± 0.003[a,b]	0.003
Tb.Sp (mm)	0.269 ± 0.010	0.237 ± 0.014	0.304 ± 0.011[b]	0.005
Conn.D (mm^{-3})	57 ± 5	97 ± 9[a]	64 ± 7[b]	0.003
DA	1.76 ± 0.02	1.83 ± 0.04	1.81 ± 0.02	0.240
SMI	-0.07 ± 0.06	0.53 ± 0.2[a]	0.99 ± 0.08[a,b]	< 0.001
TMD (mg HA/cm^3)	1229 ± 7	1198 ± 6[a]	1194 ± 9[a]	0.011
Ct.M (%)	70 ± 1	59 ± 3[a]	71 ± 2	0.006
Vertebral height (mm)	4.04 ± 0.07	4.32 ± 0.10	4.29 ± 0.07	0.220
Ulna				
Bone mass, BMC (mg)	38.5 ± 1.2	45.4 ± 0.6[a]	43.7 ± 1.2[a]	< 0.001
I_{ap} (mm^4)	0.25 ± 0.02	0.24 ± 0.01	0.24 ± 0.02	0.849
$I_{ap\text{-}avg}$ (mm^4)	0.26 ± 0.02	0.27 ± 0.01	0.26 ± 0.02	0.702
I_{ml} (mm^4)	0.65 ± 0.03	1.13 ± 0.07[a]	1.07 ± 0.05[a]	< 0.001
$I_{ml\text{-}avg}$ (mm^4)	0.82 ± 0.03	1.47 ± 0.07[a]	1.28 ± 0.07[a]	< 0.001
Section modulus, (mm^3)	0.38 ± 0.02	0.39 ± 0.02	0.40 ± 0.02	0.741
TMD (mg HA/cm^3)	1293 ± 12	1253 ± 7[a]	1234 ± 6[a]	< 0.001

[a] $p < 0.05$ *vs.* control by posthoc test

[b] $p < 0.05$ *vs.* obese by posthoc test

Table 3

Tissue material properties of right and left ulnae determined by 3-point bending and uniaxial tension (mean ± SEM).

	Lean (*n* = 6 rats)	Obese (*n* = 6 rats)	Diabetic (*n* = 6 rats)	ANOVA *p*-value
3-point bending †				
Tissue modulus (GPa)	18.3 ± 0.7	18.5 ± 0.6	15.4 ± 0.8[a,b]	0.013
Yield stress (MPa)	251 ± 2	245 ± 14	182 ± 11[a,b]	0.003
Ultimate stress (MPa)	280 ± 5	276 ± 7	246 ± 9[a,b]	0.015
Uniaxial tension				
Tissue modulus (GPa)	18.1 ± 1.6		14.8 ± 1.3	0.141
Yield stress (MPa)	79 ± 10		72 ± 10	0.631
Yield strain (%)	0.33 ± 0.02		0.25 ± 0.02[a]	0.018
Ultimate stress (MPa)	92 ± 10		92 ± 12	0.792
Ultimate strain (%)	1.30 ± 0.05		0.89 ± 0.04[a]	0.022

† Tissue material properties from 3-point bend tests were derived using beam theory equations; strain derivations are only valid in the pre-yield region of the stress-strain curve, so yield and post-yield strains are not reported

[a] $p < 0.05$ *vs.* control by posthoc test

[b] $p < 0.05$ *vs.* obese by posthoc test